RSC Advances

PAPER

Cite this: *RSC Adv.*, 2020, **10**, 27615

A microscopic and macroscopic investigation of the adsorption of N719 dye on ZnO nanopowders (ZNP) and ZnO nanorods (ZNR) for dye sensitized solar cells using statistical physics treatment and DFT simulation

Marwa Ben Manaa, *[a] Noureddine Issaoui,[a] Youssef O. Al-Ghamdi,[b] Hafedh Belmabrouk [cd] and Abdelmottaleb Ben Lamine[a]

Received 21st April 2020
Accepted 13th July 2020

DOI: 10.1039/d0ra03581e

rsc.li/rsc-advances

In this paper, three adsorption isotherms of **N719** dye on two different adsorbents, ZnO nanopowder and ZnO nanorods, at three different thicknesses have been fitted using a monolayer model with three types of receptor sites treated by statistical physics. The model involved parameters are: three coefficients (n_1, n_2 and n_3) indicating the numbers of adsorbed dye molecules per site, three parameters (N_{m1}, N_{m2} and N_{m3}) indicating the receptor site densities and three adsorption energies (($-\varepsilon_1$), ($-\varepsilon_2$) and ($-\varepsilon_3$)). The evolution of these parameters in relation with thickness of ZnO was discussed. The pore size distribution (PSD) of ZnO nanopowder and ZnO nanorods as a function of the thickness has been studied using the chosen adequate model. The molecular electrostatic potential (MEP) has been investigated to optimize the different adsorbed geometries of the complex **N719** dye@ZnO. The intermolecular interactions between the **N719** dye and the ZnO surface have been studied by using the quantum theory of atoms in molecules (AIM) and reduced density gradient RDG. The results of the MEP, topological AIM and RDG are in agreement with the results of statistical physics

1. Introduction

Dye-sensitized solar cells (DSSCs) are attracting widespread research areas and commercial interest due to the low-cost harvest of solar energy using sustainable and environmentally friendly materials.[1] DSSCs consist of a TiO_2 electrode adsorbed dye, an electrolyte solution, and a platinum counter electrode. In this class of cells, the TiO_2 electrode plays a main role in relation to the loading dye and in separating and transporting electrons.[2,3] In the assembly of DSSCs, the dye plays a key role in absorbing sunlight and converting solar energy to electrical energy with the aid of a semiconducting photoanode.[4,5] Therefore, the cell performance is mainly dependent on the type of dye used as a sensitizer.[6] Numerous metal complexes and organic dyes[4,5] have been synthesized and used as sensitizers. Ruthenium-based complexes are considered as good sensitizers for DSSCs because of their intense charge transfer absorption over the entire visible range and highly efficient metal to ligand charge transfer.[7] TiO_2 has been one of the most widely studied semiconducting materials and it has been used for DSSCs due to not only its photochemical and photoelectrochemical properties but also to its low-cost, its availability, and its non-toxic nature.[8,9] Besides TiO_2 and ZnO have been also investigated as an electron conducting material (electrode) in DSCs. It has a band gap energy and a conduction band that are similar to TiO_2.[9] It should be also noted that films of ZnO have been shown to have 2 orders of magnitude higher electron mobility than TiO_2, (110 $cm^2\ V^{-1}\ s^{-1}$ comparing to 0.01–1 $cm^2\ V^{-1}\ s^{-1}$) an important factor in DSSC performance.[10,11] Based on these characteristics, ZnO should be a promising photoelectrode material in DSC applications. Among the different techniques used to grow ZnO thin films, such as magnetron and RF magnetron sputtering, pulsed laser deposition and metal–organic chemical vapor deposition, electrophoretic deposition (EPD) are gaining increasing interest, due to its versatility and high potential for scaling up to large volumes.[12,13]

Moreover, the electrophoretic deposition (EPD) method is a well known technique for obtaining highly uniform films with thickness from the nanometer to micrometer scale by changing the applied voltage and deposition time[14,15] which has been used for coating a variety of materials.[16] Hence, this technique is suitable for fabricating thin-films for DSSCs because it allows to

[a]*Laboratory of Quantum and Statistical Physics, LR18ES18, University of Monastir, Faculty of Sciences, Monastir 5079, Tunisia. E-mail: ben.manaa.marwa@gmail.com*
[b]*Department of Chemistry, College of Science at Zulfi, MajmaahUniversity, Al Majmaah 11952, Saudi Arabia*
[c]*Department of Physics, College of Science at Zulfi, MajmaahUniversity, Saudi Arabia*
[d]*Laboratory of Electronics and Microelectronics, Faculty of Science of Monastir, University of Monastir, Tunisia*

control the film thickness of photoelectrode which is critical to cell efficiency.

In addition, previous studies have shown that, in the dye sensitized solar cells, only chemisorbed dye molecules can inject electrons into the electrode material indicating just only the first layer of dye molecules is effective.[17,18] However, multilayers of dye can absorb incident light but cannot inject the electrons to the photoelectrode. Therefore, it would be better to optimize the adsorbed dye for further improving performance. A more accurate way for determining whether dye monolayers or multilayers are formed is by employing direct methods. There are few experimental techniques that offer direct information about the ZnO interface structure and the **N719** ruthenium-based dye such as using the photoelectron spectroscopy (PES) technique,[19] this method has been performed also on dye-sensitized ZnO electrodes to study the **N719** and Z-907 dyes coverage and the anchoring to the ZnO surface. This technique has indicated that the adsorbed **N719** dye on ZnO film is a multilayer process in a specific experimental conditions.[19] In addition, Neutral Impact Collision Ion Scattering Spectroscopy (NICISS) is also an experimental direct technique which has been used with the standard indirect solution depletion method to investigate the adsorbed layer of **N719** dye on titanium oxide.[20] Previously, the combination of both direct experimental techniques AFM and Neutral Impact Collision Ion Scattering Spectroscopy (NICISS) allowed conclusions to be drawn about the thickness and homogeneity of the adsorbed dye layer.[21] Various theoretical method based on quantum chemistry calculation has provided the valuable reference for predicting the relationship between the structure and photoelectrical properties of molecules for dye sensitized solar cells.[22,23] Ben Lamine *et al.*[24] have developed a statistical physics treatment based on quantum physics theory which is useful to interpret various adsorption systems.[25,26] Marwa *et al.*[27–31] have improved this theory and developed new statistical physics models for modeling adsorption isotherms of dyes for DSSCs applications. Recently, to investigate the optical properties of DSSCs, theoretical methods as computational simulations rooted in density functional theory (DFT) and time-dependent DFT (TDDFT) have become a crucial tool to understand the detailed atomistic and the interatomic interactions that are more necessary to the complex dye/semiconductor interaction.[32,33] Therefore, it is necessary to combine the statistical physics and DFT approaches to be used as an efficient predictive tool in studies of DSSCs optimization. In this context, studies on dye-sensitized ZnO models are however scarce (see, for example, ref. 34 and 35) and to the best of our knowledge, the interaction of the prototypical **N719** Ru(II) dye with ZnO has never been reported using these both approaches. In order to fill this void, we present here a statistical physics formalism to describe in the macroscopic level the adsorption process of the **N719** dye into the ZnO surface. The analytical expressions have been developed by the statistical physics theory to model the adsorption isotherms of **N719** dye into ZnO nanopowders (ZNP) and ZnO nanorods (ZNR) at different thickness of EPD films. These films ZNP and ZNR were fabricated by an electrophoretic deposition technique (EPD) at three deposition time $t_1 = 1$ min, $t_2 = 3$ min and $t_3 = 5$ min. The variation of adsorbent thickness represents an important parameter which has a strong influence on the evolution of the adsorption process. The statistical physics modeling gives physico–chemical parameters that are involved in these analytical expressions. With these parameters (adsorption energy, stoichiomtric coefficients, number of layers and receptor sites density), the adsorption process description is becoming very significant. While the DFT simulation has been used to study the interatomic interaction between the

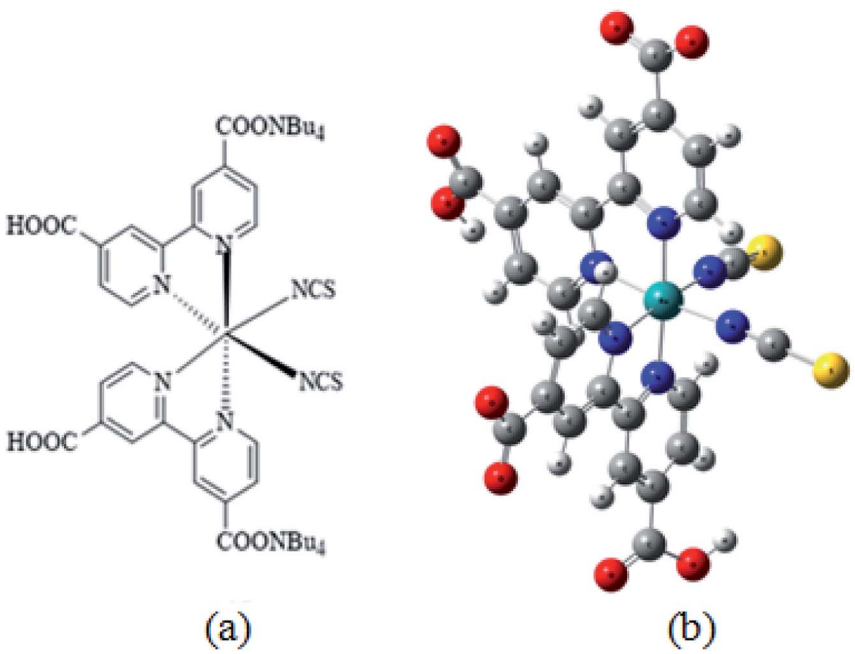

Fig. 1 Chemical structure of **N719** dye (a) and (b) the optimized structure of **N719** dye determined by the DFT simulation.

prototypical **N719** dye and the ZnO nanostructure. We pay particular attention to the adsorption modes, geometries and energies. At the first time, the optimization of adsorbed geometries of the complex **N719** dye@ZnO have been carried out by a molecular electrostatic potential (MEP) to predict reactive sites for electrophilic and nucleophilic attack and the interaction energies have been investigated by using the topological AIM and reduced density gradient RDG.

2. Material and methods

2.1 Adsorbate

The adsorbate is a **N719** dye (Ruthenizer 535-bisTBA) was purchased from Solaronix.[36]

The chemical structures of the **N719** dye are illustrated in Fig. 1

2.2 Adsorbent

ZnO nanopowders (Sigma-Aldrich, hereafter denoted ZNP) were purchased and used without further purification. ZnO nanorods (hereafter denoted ZNR) were fabricated from 0.3 M ZnO sols treated by solvothermal synthesis (150 °C for 5 days).[35,36]

2.3 Adsorption isotherms

The fabricated ZnO films whose area was 0.5 cm^2 (photoelectrodes; PE) were soaked in 0.05, 0.15, 0.2, 0.3, and 1.0 mM of an ethanolic **N719** (Solaronix) dye solution for 30 min, followed by rinsing with dry EtOH (C_2H_5OH, clear leader) and letting them dry. The UV-Vis spectroscopy (UV-2401, Shimadzu) has been used to determine the amount of dye loaded onto the films.[36] Then, the films loaded with dye where then soaked in 0.1 M NaOH mix solution of water/ethanol (1 : 1, v/v) to desorb the dye, and the absorption of spectrum of samples has been measured.

The adsorption isotherms of **N719** dye on ZnO nanopowders (ZNP) and ZnO nanorods (ZNR) at different thickness of EPD films are illustrated in Fig. 2.[36]

3. Theory of statistical physics treatment

Adsorption process involves an exchange of particles from the dissolved free state to the adsorbed state. Its investigation by statistical physics formalism cannot be performed without employing the grand canonical ensemble to take account of the particle number variation through the introduction of the chemical potential variable in the adsorption process.[24,37] Theoretical modeling of adsorption isotherms in gas or liquid phase based on statistical physics development is a powerful technique used for surface characterization. One of the advantages of applying this theory is to give a physicochemical meaning to the parameters involved in the model and then to provide new interpretations of the adsorption process at molecular level. In order to treat the adsorption process by using the statistical physics methods, certain hypotheses were considered as a basis of the corresponding treatment and applied to facilitate the calculations as well as interpretations. At a first approximation, the interaction between the dye molecules was neglected, the internal degrees of freedom of the studied molecules are also neglected and we except the translation freedom degrees. Indeed, the electronic degrees of freedom cannot be thermally excited. The rotational freedom degrees could be considered as are frozen in the solution. Finally, the vibrationel freedom degrees can be neglected at first approximation at room temperature.

According to these assumptions, in the liquid phase, the adsorption reaction of a dye molecule (D) onto a receptor site (S) should include a stoichiometric coefficient n as expressed in the following equation:

$$nD + R \leftrightarrows D_nR \quad (1)$$

where n represents the number of adsorbed dye molecules per site D and D_nR is the formed dye–ZnO complex.

In this treatment, the starting point, is the use of the grand canonical partition function which describes the system microscopic states in the adsorption process.

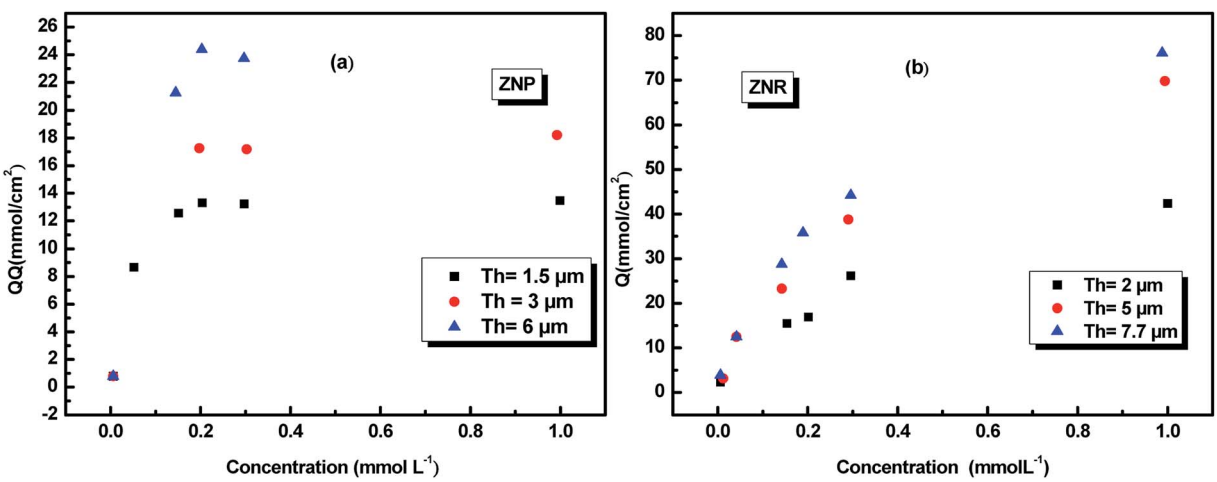

Fig. 2 Adsorption isotherms of **N719** dye on ZNP and ZNR materials at different thickness of EPD films.[36]

The grand canonical partition function of one receptor site can be expressed as:

$$z_{gc} = \sum_{N_i} e^{-\beta(-\varepsilon-\mu)N_i} \quad (2)$$

where $(-\varepsilon)$ is the receptor site adsorption energy, μ is the chemical potential, N_i is the receptor site occupation state, and $ß$ is defined as $1/k_B T$, where k_B is the Boltzmann constant and T is the absolute temperature.

The total grand canonical partition function related to N_m receptor sites per unit mass is written as follows:

$$Z_t = (z_{gc})^{N_m} \quad (3)$$

The average site occupation number N_o can be derived from the total grand canonical partition function:[24,37]

$$N_o = \frac{1}{\beta}\frac{\partial \ln Z_t}{\partial \mu} = N_m K_B T \frac{\partial \ln z_{gc}}{\partial \mu} \quad (4)$$

For n molecules anchored per site, the total number of adsorbed molecules Q is given by:

$$Q = nN_o \quad (5)$$

The analytical expression Q is calculated by considering a given starting a given staring partition function. Now we have to choose plausible model analytical expressions from the literature which susceptible to best fit the experimental adsorptions isotherms curves. Taking account of the isotherms forms, the experimental curves have been fitted with the conventional model Langmuir and with the six proposed statistical physics models: a monolayer model with one energy (Model 1), a monolayer model with two energies (Model 2), monolayer model with three energies (Model 3), a monolayer model with four energies (Model 4), a double layer with one energy (Model 5) and a double layer with two energies (Model 6). We established analytical expressions corresponding to the adsorption isotherms **N719** on ZNP and ZNR materials on the basis of statistical physics treatment. In the next section, we developed with details the adequate grand canonical partition function, and afterward the analytical expression of the best fitting model.

All the expressions of the others treated models are given in the Appendix.

3.1 Development of the best fitting model: the monolayer model with three types of sites

This model is an extended Hill model but with three different types of receptor sites taking into account of the heterogeneity of ZNP and ZNR surfaces. To develop this model by using the grand canonical ensemble in statistical physics, we supposed that the adsorption process occurs onto three types of sites characterized by three different adsorption energies ($-\varepsilon_1$, $-\varepsilon_2$ and $-\varepsilon_3$). The value of the adsorption energy is characteristic of the receptor site with a density of receptor sites noticed N_{m1}, N_{m2} and N_{m3}. One receptor site is supposed to be empty or occupied by one or more dye molecules.

The first step to establish this model is to express the grand canonical partition function of one receptor site describing the microscopic states of the adsorbing system. Therefore, the grand canonical partition functions of one site of the three types are expressed by the following relations:

$$z_{1gc} = \sum_{N_i=0,1} e^{-\beta(-\varepsilon_1-\mu)N_i} = 1 + e^{\beta(\varepsilon_1+\mu)} \quad (6)$$

$$z_{2gc} = \sum_{N_i=0,1,2} e^{-\beta(-\varepsilon_2-\mu)N_i} = 1 + e^{\beta(\varepsilon_2+\mu)} \quad (7)$$

$$z_{3gc} = \sum_{N_i=0,1,2,3} e^{-\beta(-\varepsilon_3-\mu)N_i} = 1 + e^{\beta(\varepsilon_3+\mu)} \quad (8)$$

with z_{1gc}, z_{2gc} and z_{3gc} being the partition functions of the three types of the site.where μ are the chemical potential son site, respectively and N_i is the number of occupation.

Therefore, the total partition function of the monolayer model of three receptor sites is:

$$Z_t = (z_{1gc})^{N_{m1}}(z_{2gc})^{N_{m2}}(z_{3gc})^{N_{m3}} \quad (9)$$

Using the previous definition of occupation number, the each average number of occupied sites is:

$$N_{o1} = \frac{N_{m1}}{1+\left(\frac{C_1}{C}\right)^{n_1}},\quad N_{o2} = \frac{N_{m2}}{1+\left(\frac{C_2}{C}\right)^{n_2}},\quad N_{o3} = \frac{N_{m3}}{1+\left(\frac{C_3}{C}\right)^{n_3}}$$

The total number of adsorbed dye molecules Q is:

$$Q = n_1 N_{o1} + n_2 N_{o2} + n_3 N_{o3} \quad (10)$$

Finally, Q is the number of adsorbed molecules of dye *versus* the concentration C is:

$$Q = \frac{n_1 N_{m1}}{1+\left(\frac{C_1}{C}\right)^{n_1}} + \frac{n_2 N_{m2}}{1+\left(\frac{C_2}{C}\right)^{n_2}} + \frac{n_3 N_{m3}}{1+\left(\frac{C_3}{C}\right)^{n_3}} \quad \text{Model 3}$$

with C_1, C_2 and C_3 being the concentrations at half saturation for the first type, the second type and the third type of receptor sites respectively.

4. Results and discussion

4.1. Best fitting model choice

Experimental data were analyzed by non-linear curve fitting analysis, using Microcal Origin Lab software (Origin Lab, Northampton, MA), to fit our adsorption isotherm with the different statistical physics models presented in the previous sections. The fitting goodness of each model was discussed in terms of different error functions. The best fitting adsorption isotherm was determined by the well-known correlation coefficient R^2 and the analysis of the residual root mean square error (RMSE) called as the estimated standard error of the regression. They are the most popular used method to determine the optimum isotherm.

The correlation coefficient R^2 was calculated using the following equation:

$$R^2 = 1 - \left(\left(1 - \frac{\sum_i^m (Q_{i,\mathrm{exp}} - \overline{Q}_{i,\mathrm{exp}}) - \sum_i^m (Q_{i,\mathrm{Exp}} - \overline{Q}_{i,\mathrm{model}})}{\sum_i^m (Q_{i,\mathrm{Exp}} - \overline{Q}_{i,\mathrm{exp}})} \right) \times \frac{n_\mathrm{p} - 1}{n_\mathrm{p} - p} \right) \quad (11)$$

where, $Q_{i,\mathrm{exp}}$ is each value of Q measured experimentally, $Q_{i,\mathrm{model}}$ is each value of Q estimated by the fitted model, Q_{exp} is the average of Q experimentally measured, n_p is the number of performed experiments and p is the number of parameters of the fitted model.

For a number p of adjustable parameters, the estimated standard error is given by the following relation.[38]

$$\mathrm{RMSE} = \sqrt{\frac{\mathrm{RSS}}{m' - p}} \quad (12)$$

where RSS is the residual sum of squares and m' is the number of experimental data.

In Table 1 we present the adjustment correlation coefficient of the seven treated model at three different thicknesses.

RMSE

Studied system	Th (μm)	Langmuir	Model 1	Model 2	Model 3	Model 4	Model 5	Model 6
ZNP	**1.5**	0.41	0.01	0.03	0.003	0.022	0.341	0.231
	3	0.31	0.42	0.071	0.006	0.03	0.111	0.453
	5	0.62	0.8	0.05	0.009	0.053	0.134	0.521

(*Contd.*)

RMSE

Studied system	Th (μm)	Langmuir	Model 1	Model 2	Model 3	Model 4	Model 5	Model 6
ZNR	**2**	0.03	0.32	0.232	0.001	0.04	0.120	0.211
	6	0.52	0.66	0.211	0.003	0.023	0.452	0.143
	7.7	0.83	0.543	0.273	0.002	0.034	0.321	0.121

The Table 1 shows that the coefficient correlation R^2 of the model 3 are close to the unity and its values of RMSE are close to zero in comparison of the other tested models. Indeed, the monolayer model with three energies is considered as the adequate model to describe the adsorption process of **N719** dye on the two materials ZNP and ZNR. In addition, to R^2 and RMSE coefficients criteria, our choice has also taken into account the physics justification in model selection. If the monolayer model of three energies is chosen as the best fitting model, it would provide the best description of the adsorption data of **N719** dye on ZNP and ZNR materials. All its adjusting parameters are reported in Table 2.

The adsorption equilibrium data for **N719** dye on ZNP and ZNR fitted by the adequate model are reported in Fig. 3.

The physicochemical model parameters have a main role to describe with detail the adsorption process at a molecular level. They give more details of the adsorption process allowing a careful description of the dynamic and the steps of the absorption process.

The different fitted parameters are classified in two categories: stereographic and energetic parameters. The stereographic parameters are the numbers of adsorbed dye molecules

Table 1 Adjustment coefficient R^2 and RMSE for each model

R^2

Studied system	Th (μm)	Langmuir	Monolayer with one energy	Monolayer model with two energies	Monolayer model with three energies	Monolayer model with four energies	Double layer with one energy	Double layer with two energies
ZNP	**1.5**	0.95	0.987	0.998	0.999	0.978	0.877	0.756
	3	0.97	0.898	0.978	0.998	0.897	0.885	0.873
	5	0.96	0.856	0.988	0.989	0.987	0.897	0.876
ZNR	**2**	0.89	0.78	0.69	0.999	0.87	0.676	0.765
	6	0.76	0.88	0.87	0.989	0.889	0.778	0.887
	7.7	0.77	0.87	0.89	0.999	0.899	0.855	0.654

Table 2 Fitting parameters of experimental data of Fig. 1(a) and (b) with the model 3

Adsorbent	Th (μm)	n_1	n_2	n_3	N_{m1} (mmol cm^{-2})	N_{m2} (mmol cm^{-2})	N_{m3} (mmol cm^{-2})	Q_{sat1} (mmol cm^2)	Q_{sat2} (mmol cm^{-2})	Q_{sat3} (mmol cm^{-2})
ZNP	1.5	0.4	1.4	2.7	0.4	1.5	2	0.16	2.1	5.4
	3	0.9	1.9	3.2	0.8	2	2.4	0.72	3.8	7.68
	6	1.2	2.4	3.7	1.2	2.4	3	1.44	5.76	11.1
ZNR	2	0.6	3.2	6.4	0.8	2.5	4	0.48	8	25.6
	5	1.4	4.3	7.3	1.5	3	4.2	2.1	12.9	30.66
	7.7	2.5	5	8.4	2.2	3.2	4.6	5.5	16	38.64

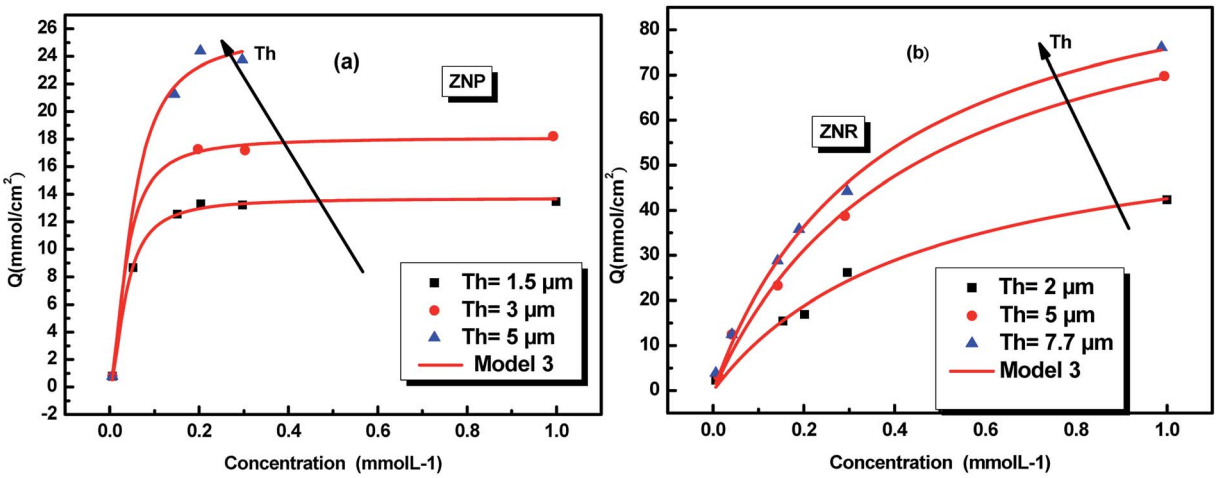

Fig. 3 Fitted adsorption isotherms of **N719** dye on ZnO nanopowder (ZNP) (a) and on ZnO nanorods (ZNR) (b) at different thickness of (EPD) film: the squares, circles and triangles are the experimental data[36] and the continuous red lines are the simulated data.

per site n_1, n_2 and n_3. These numbers represent the stoichiometric parameters. They give also the geometric properties of the studied aggregates, such as their orientation and their sizes. The densities N_{mi} are also geometric indication of the sites repartition. The second category of parameters is energetic. They represent the halves-saturation concentrations C_1, C_2 and C_3 which allow to calculate the adsorption energies in order to identify the kind of the anchorage of **N719** dye on the ZNP and ZNR materials.

4.2. Stereographic interpretations

4.2.1 The parameters n_1, n_2 and n_3. The parameters n_1, n_2 and n_3 in the adsorption reaction eqn (13)–(15) represent the stoichiometric coefficients, and they represent also the number of adsorbed dye molecules per site given in the expression of the model 3.

The reaction eqn (1) can be replaced using model 3 by three reactions eqn (13), (14) and (15).

The reaction in the first site is written as:

$$n_1\mathrm{D} + R \leftrightarrows \mathrm{D}n_1R \quad (13)$$

The reaction in the second site is written as:

$$n_2\mathrm{D} + R \leftrightarrows \mathrm{D}n_2R \quad (14)$$

The reaction in the third site is written as:

$$n_3\mathrm{D} + R \leftrightarrows \mathrm{D}n_3R \quad (15)$$

This parameter can also give information on the positions of the adsorbed molecule at the adsorbent surface sites. In fact, a molecule has several manners to be anchored on the receptor site according to its geometry and its angle of incidence with the adsorbent surface.

In general, the n parameter plays two main roles: one hand, it describes geometrically the adsorption position of dye on the adsorbent surface as function of their values determined by numerical simulation. Other hand, describes the aggregation phenomena and their degree of the adsorbate molecules in solution.[37] According to the adsorption position of the dye, it can be distinguished two possible configurations relative to the surface: in the first case, if this value is superior to 1, it represents the number of docked molecules which interact with one receptor site describing a multi-molecular process. This describes the case that the dye molecules are anchored by a gathered n dye molecules on the adsorbent surface as an aggregate or a linear polymer. In the second case, if this value is inferior to 1, it would represent "the fraction of the dye per site", leading to a horizontal docking[37,38] on the adsorbent surface and showing that the adsorption is multi-docking process.[37,38] Then $n' = 1/n$ represents the anchorage number of one dye molecule on an average number of receptor sites.[37,38] Referring to the values of this parameter (Table 2), we noticed that there are values superior to the unity and others are inferior at a time.

In order to simplify the description, let's consider an example in the case of adsorption of **N719** dye on ZNP film a value of n which is superior to the unit: $n_2 = 1.4$ at applied thickness of (EPD) = 1.5 μm. We can write $1.4 = 1 \times x + (1 - x) \times 2$. A rate of 60% receptor sites are docked by one molecule and 40% of receptor sites are occupied by two molecules of **N719** dye with a non parallel position. However, in the case of adsorption of **N719** dye on ZNR film, we noticed different behaviors with $n_1 > 1$ and $n_1 < 1$. For $n_1 < 1$ let's take this case when $n_1 = 0.6$. The dye **N719** is anchored on the surface of ZNR with at least two different manners. This value can be considered as an average between 1/2 and 1. Therefore, we can describe it by this relation $0.6 = x \times 1 + (1 - x) \times 1/2$ enables to calculate the percentage values of single docked molecule ($x = 40\%$) and double docked one ($1 - x = 60\%$). Moreover, from the Table 2, we noticed that the different thickness of EPD films has a noticed influence on the stereography of the adsorption process or on the variation of the number of adsorbed dye molecules on the ZNP and ZNR films. Indeed, we reported in Fig. 4 the evolution of the numbers of dye molecules per site calculated with model 3 as function of the thickness of EPD films.

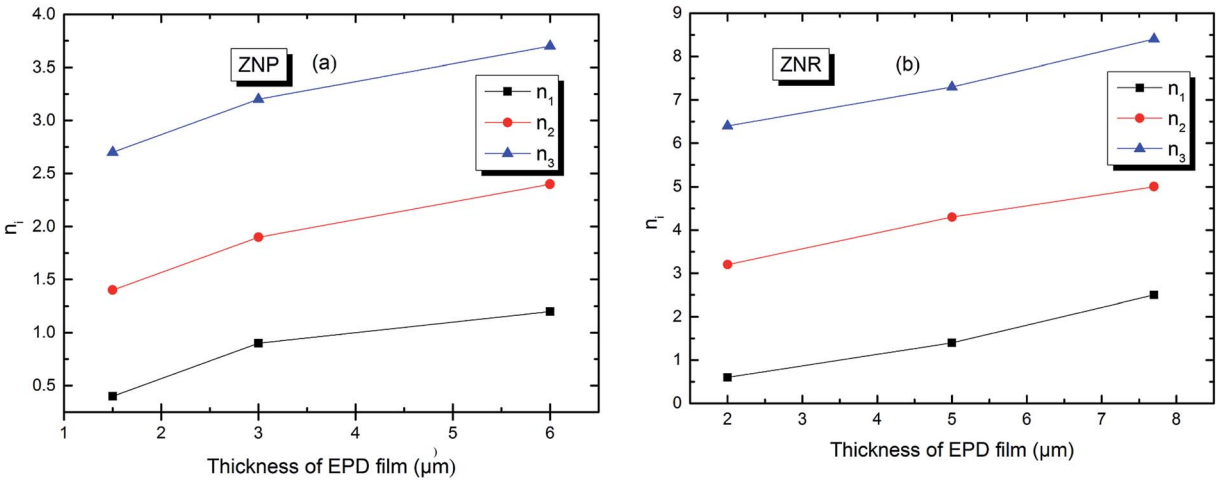

Fig. 4 Numbers of adsorbed dye molecules per sites n *versus* the thickness of EPD films: (a) ZNP and (b) ZNR.

Table 3 Values corresponding to the adsorption energies of the three adsorption sites in ZNP and ZNR materials at different thickness of EPD films

Studied system	Thickness of EPD film (μm)	C_1 mol L^{-1}	C_2 mol L^{-1}	C_3 mol L^{-1}	$-\varepsilon_1$ kJ mol^{-1}	$-\varepsilon_2$ kJ mol^{-1}	$-\varepsilon_3$ kJ mol^{-1}
ZnO (ZNP)	**1.5**	5×10^{-11}	8×10^{-11}	0.2×10^{-11}	58.76	57.60	66.740
	3	6×10^{-13}	2×10^{-13}	0.5×10^{-13}	69.72	72.44	79.86
	6	5×10^{-14}	2×10^{-14}	1×10^{-14}	75.87	78.15	85.56
ZnO (ZNR)	**2**	0.5×10^{-7}	4×10^{-8}	2×10^{-8}	41.64	42.19	43.91
	5	0.8×10^{-9}	0.2×10^{-9}	0.5×10^{-10}	52	55.33	58.76
	7.7	2×10^{-11}	0.9×10^{-11}	0.4×10^{-11}	61.03	63.01	65.02

The Fig. 4 shows first of all, that the numbers of adsorbed dye molecules n_i increase with the increase of the thickness of (EPD) for a given fixed type of sites. This can be explained that the increase in thickness leads to an increase of the attraction to the dye molecule. This can be expressed by an increase of an attraction mean field, synonym of an increase of the adsorption energy (Fig. 7 and Table 3) and consequently an increase of chemical potential through the increase of n_i. The Fig. 4 shows also, that for a given thickness, the n_i is increased conventionally from the first type of sites till the last type or the third type of sites. But in reality, the more energetic site will be the first to be kinetically occupied. So the third type of sites will be the first occupied, followed by the second and so on. We see from the Fig. 4 that the third and the second types are multimolecular adsorption process or dye aggregation adsorption process. The first type or the last occupied or the less energetic, becomes

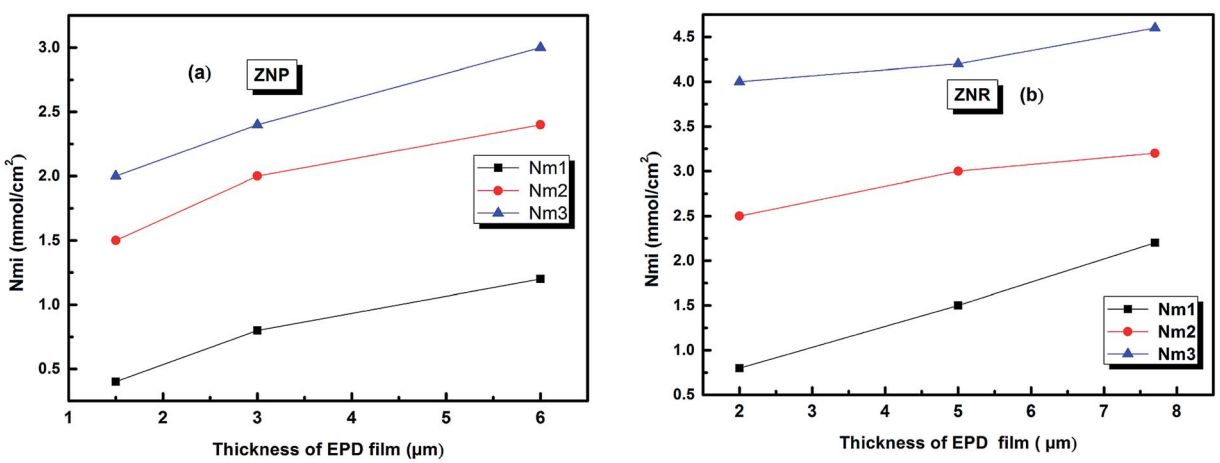

Fig. 5 The evolution of the densities of receptor site *versus* the thickness of EPD films. (a) ZNP and (b) ZNR.

a multianchorage adsorption process $n_1 \leq 1$. Finally, comparing Fig. 4(a) and (b) we notice that the features of the adsorption process in ZNP and ZNR are similar. However, due to the energetic aspect and so to the aggregation parameter n_i which are better in ZNR then ZNP leading to the an amelioration of the adsorption capacity defined by the following relation

$$Q_{sat} = \sum_{i=1,3} n_i Q_i \quad (16)$$

4.2.2 Density of receptor sites N_{mi}. These steric parameters N_{mi} describe the effectively occupied receptor sites when the saturation is reached.

The variation of the receptor sites densities N_{mi} *versus* the thickness of EPD films is reported in Fig. 5.

The Fig. 5 shows that the densities N_{mi} increase with an increase of (EPD) films thickness. This is probably related to the increase in the adsorption energy caused by an increase of the thickness. This thickness gives a medium confinement leading to a reinforcement of the aggregation process in one hand, but also to a reinforcement of the accessibility of additional adsorption receptor sites for the **N719** dye molecules in another hand. Therefore the **N719** dye molecules can be easily fixed onto the adsorbent surface.

4.2.4 The amount of adsorbed molecules at saturation Q_{sati}. The parameter Q_{sati} represents the total saturation adsorbed quantity of the studied system. This quantity is very useful to determine the specific area of samples. Indeed, it depends on the number of molecules per site n_i and the density of receptor sites N_{mi} by the following relation:

$$Q_{sati} = Q_{sat1} + Q_{sat2} + Q_{sat3} = \sum_{i=1}^{3} Q_{sati} \text{ and } Q_{sati} = n_i N_{mi}$$

The evolution of this parameter as a function of the thickness of EPD films is reported in Fig. 6

From (Fig. 6a and b), we noticed that the values of $Qsat_i$ increased with the increase of thickness of (EPD) films both on ZNR and ZNP materials. These behaviours are consequently attributed to the two increases of the densities of receptor sites N_{mi} and to the molecules numbers n_i per site cited in the Table 2. Moreover, the amount of adsorbed dye increased with film thickness due to the same reasons. However, the higher saturated adsorbed quantity per unit of surface onto films of ZNR can be attributed to the higher values of n_i (Fig. 4(a)), and N_{mi} (Fig. 5(a))

5. Adsorption energies

In order to investigate the type of interaction between the **N719** dye molecule and ZNP and ZNR materials, we calculated the adsorption energies of the dye molecule using the following expressions:

$$-\varepsilon_1 = RT \ln\left(\frac{C_s}{C_1}\right) \quad (17)$$

$$-\varepsilon_2 = RT \ln\left(\frac{C_s}{C_2}\right) \quad (18)$$

$$-\varepsilon_3 = RT \ln\left(\frac{C_s}{C_3}\right) \quad (19)$$

where R is the ideal gas constant, $R = 8.314$ J (mol K)$^{-1}$ and C_s is the solubility or the saturation concentration of dye. All the calculated adsorption energies values are reported in the Table 3.

From the Table 3, we deduce that the value of adsorption energies $(-\varepsilon_1)$, $(-\varepsilon_2)$ and $(-\varepsilon_3)$ of the dye molecules adsorbed chemically on the ZNP surface and ZNR surface since the obtained values were superior than 40 KJ mol^{-1}.[39] Therefore, these values mean that the carboxylic group of **N719** dye is chemically bond on the ZNP and the ZNR materials.

Indeed, the carboxylate groups provide a strong adsorption of the dye on the ZNR and the ZNR surface, thus fully justifying by involving valency forces through the exchange of electrons between dye molecules and ZnO nanorods ZNP and ZnO nanorods ZNR as covalent forces. We reported in Fig. 7 the

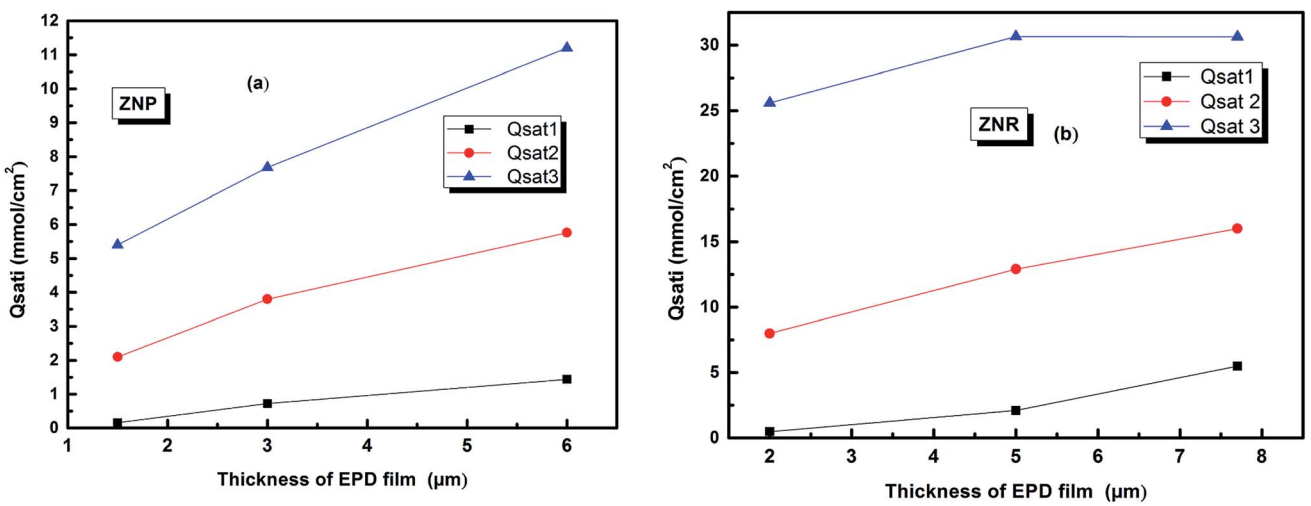

Fig. 6 The evolution of the amount of adsorbed molecules *versus* the thickness of (EPD) films. (a) ZNP and (b) ZNR.

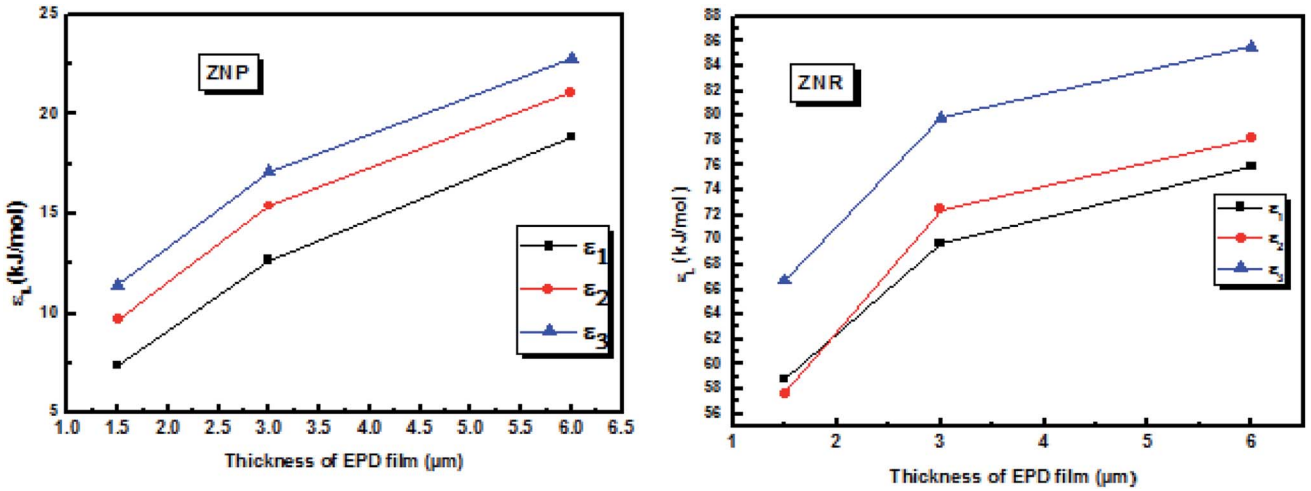

Fig. 7 Evolution of the energies of the three receptor sites as a function of thickness of EPD films.

evolution of energies of all receptor sites as a function of the different thicknesses of EPD films.

From the Fig. 7, we noticed that the value of energies increases with the increases of depositions times of ZNP and ZNR materials. This increase attributed to the increase of thickness of the adsorbents, can be easily attributed to the anchorage of **N719** dye *via* carboxylic groups. According to the our previous results about the adsorption of the different models of **N719** on nanoporous TiO_2 (ref. 27) in the case of the adsorption **N719** dye on ZNP and ZNR, we figure out three possible configurations in Fig. 8: three models for chemisorptions of the **N719** dye carboxylate group on ZNR and on ZNP materials.

According to the obtained values of number of adsorbed dye molecules (Table 2), we illustrate in Fig. 9 an example of chemisorption anchorage of **N719** dye *via* carboxylic group on the ZNP and ZNR respectively with hexagonal (Wurtzite) structure.[40]

6. Pore size distribution (PSD) determined by the adequate model

In this section, we characterized the adsorbent morphology by means of the PSD which describes the geometric heterogeneity of the **N719** dye on ZNP and ZNR materials at different thicknesses during the adsorption process. In general, the Barrett–Joyner–Halenda (BJH) method, the most common method available in literature has been used to determine the pore size distribution of different porous materials, though, in our work, we estimated the PSD by a new Kelvin's law relating between the pore radius r and the dye concentration C and the concentration at saturation C_s developed by Patrick *et al.*[41,42] that we previously used in (ref. 28 and 29).

The Kelvin's law is given by the following equation:

$$\ln\left(\frac{C}{C_s}\right) = \frac{-2\gamma V_m}{rRT} \quad (20)$$

The V_m is the molar volume, γ is the surface tension of the Wall with contact angle θ, T is the temperature, $R = 8.314$ is the ideal gas constant and r is the cylindrical pore radius of ZnO.

So we can write eqn (20) in the following relation:

$$\frac{C}{C_s} = e^{\frac{-2\gamma V_m}{rRT}} = e^{-\frac{K_k}{rRT}} \quad (21)$$

where C_s is the **N719** dye solubility or its concentration in solvent at saturation, $K_k = 2\gamma V_m$ is the constant of Kelvin

Substituting into eqn (9) the four relations:

$$\frac{C}{C_1} = \frac{C_s}{C_1}e^{\left(\frac{-K_k}{rRT}\right)}, \quad \frac{C}{C_2} = \frac{C_s}{C_2}e^{\left(\frac{-K_k}{rRT}\right)}, \quad \frac{C}{C_3} = \frac{C_s}{C_3}e^{\left(\frac{-K_k}{rRT}\right)}$$

we obtain an equation which relates the adsorbed quantity Q with the pore radius.

Therefore, the derivative of the adsorbed amount Q relative to the radius gives the pore size distribution of the adsorbent:[27,28]

$$\mathrm{PSD} = \frac{dQ}{dr} \quad (22)$$

The variation of this distribution for different values of the temperature is illustrated in Fig. 10

First of all, the Fig. 10 shows that both ZNP and ZNR are mesoporous. The Fig. 10(a), shows also that the pore size distribution of ZNP exhibits particularly that the adsorbent is

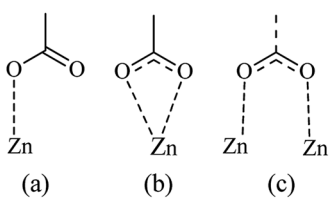

Fig. 8 Probable models for the chemisorption of the N719 dye carboxylate groups into the ZnO nanopowder surface (ZNP) and ZnO nanorods surface: (a–c) illustrate the monodentate, bidentate chelate and bidentate bridging configurations, respectively.

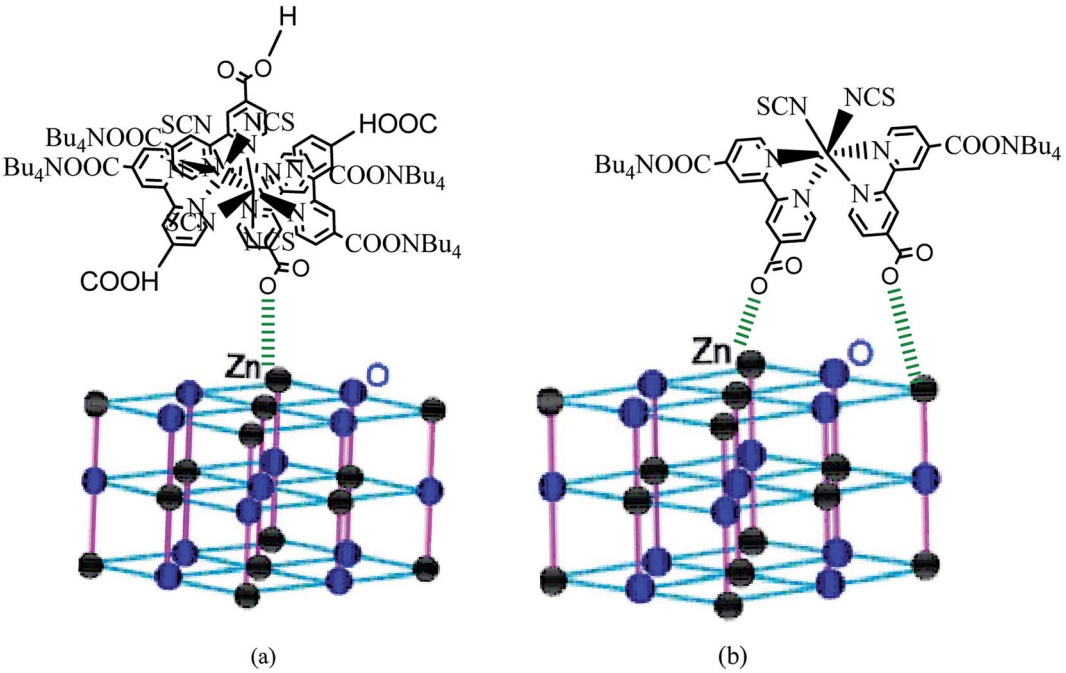

Fig. 9 An example of the carboxylic group of **N719** dye: (a) adsorbed chemically on the ZNP material *via* one carboxylic group according to the Table ($n = 1.4$ ˃ 1) and (b) adsorbed chemically on the ZNR surface *via* two carboxylic groups according to the Table 2 ($n = 0.6 < 1$) *via* one two carboxylic groups by bidentate chelate mode.

a mesoporous material with a pore radius about few nm (5 nm < r < 20 nm). However, the Fig. 10(b) shows that the adsorbent ZNR is also mesoporous material but with a large pore radius (20 nm < r < 90 nm) at applied thickness Th = 2 μm and Th = 5 μm and Th = 7.7 = μm. It is noticed that the thickness of EPD has a significant effect on the variation of the PSD of the two adsorbent materials ZNP and ZNR. The increase in thickness leads to a translation of PSD of the two materials to the higher pores.

In the next section, the DFT simulation has been used to complete the statistical physics to understand with details the molecular interaction between the **N719** dye and the ZnO material.

7. DFT simulation: study of the interaction surface between the N719 dye and the ZnO

7.1 Computational details

The molecular geometry optimization of the dye sensitizer **N719** was performed by using the B3LYP methods by means of the exchange–correlation functional and a 311++G(d,p) basis set with the Gaussian09 (G09) program package and the GaussView molecular visualization program.[43–45] The B3LYP functional has been broadly used for calculations of various organic compounds, which justifies its use for the given system.[46–48] The computational results showed the formation

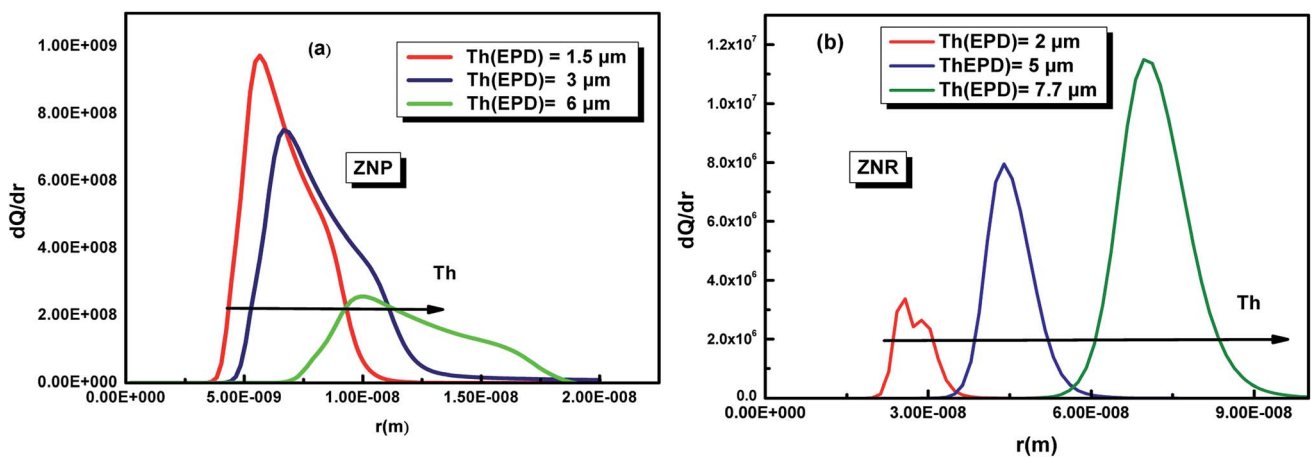

Fig. 10 Pore size distribution of the ZNP (a) and ZNR (b) materials at different thicknesses Th of EPD films.

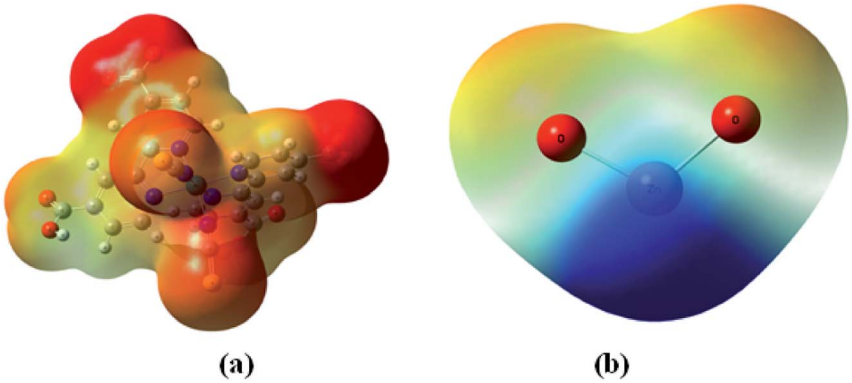

Fig. 11 The molecular electrostatic potential (MEP) map of (a) **N719** dye and (b) ZnO.

of hydrogen bonding and electrostatic interactions that suggest the increased reactivity and potential adsorption activity of these complexes. In order to estimate the different possible optimized geometries of the **N719** dye adsorbed on the ZnO nanoparticle, first of all, we are interested in studying the molecular electrostatic potential to estimate the different active sites deduced from the electrophilic attack and nucleophilic reaction.

7.2 Molecular electrostatic potential (MEP)

The molecular electrostatic potential surface (MEP) displays electrostatic potential distribution (electron and nuclei), size, dipole moments and shape of the molecule where the relative polarity can easily be visualized.[49] It is very useful to predict reactive sites for electrophilic attack and nucleophilic reactions as well as hydrogen-bonding interactions.[50,51] MEP maps can be obtained by mapping electrostatic potential onto the total electron density with color code. There are three important colors; blue, red and green used to indicate the value of the electrostatic potential. The surfaces with blue and red colors show the positive and negative values of the potential respectively. The surfaces with green colors indicate zero potential. In this study, the red, blue and green colors are used to identify the electrophilic, nucleophilic and neutral sites of **N719** dye and ZnO material.

The MEP surfaces mapped for the **N719** dye and ZnO structure by using B3LYP/6- 311++G (d,p) level are shown in Fig. 11.

From the Fig. 11 the blue color reveals the strongest attraction whereas the red color indicates the strongest repulsion.

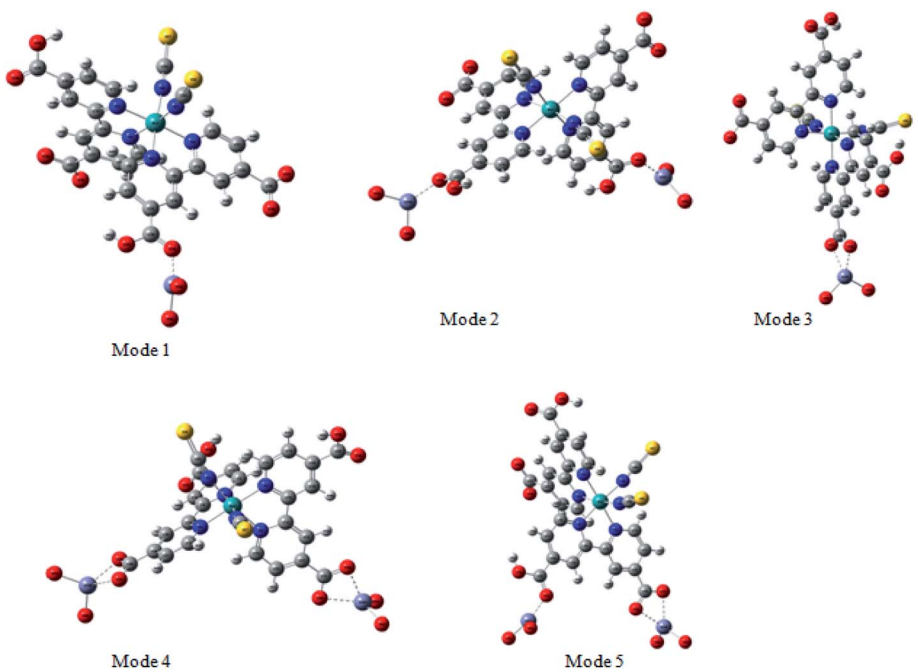

Fig. 12 Possible binding modes for **N719** dye on surface ZnO: monodentate mode *via* one carboxylic group (Mode1), bidentate bridging mode *via* both carboxylic groups (Mode 2), bidentate chelate mode *via* one carboxylate ion group –COO– (Mode 3), bidentate chelate mode *via* both carboxylate ion groups –COO– (Mode 4), bidentate bridging mode *via* one carboxylic group and one carboxylate ion group –COO– (Mode 5).

The examination of this figure shows that there is an excess in electrons in the areas of negative potentials which is associated to the four carboxylic groups of **N719** dye while the region of the positive potential (deficient in electrons) is associated to the Zn atom. This confirms the existence of five active sites between the adsorbate and the adsorbent. Indeed, these electrophilic and nucleophilic sites explain the formation of the O-bonds between the Zn atom and the carboxylic groups. The presence of this binding predicts a good stability of our system.

7.3 Adsorption modes: geometric optimization

The adsorption of the dye on the semiconductor surface is known to play a main role on the dye sensitized solar cells DSSCs.[46] Indeed, the strength of the dye/semiconductor interaction determines the stability of the nanocomposite lying at the heart of the solar cell.

In order to study much better the interatomic interactions between the **N719** dye and on the ZnO surface, a DFT simulation has been used to optimize the different adsorption geometries of the adsorbed **N719** dye on ZnO surface. A correct prediction of the adsorption geometries is an essential prerequisite to properly capture the intricate electronic structure of the dye@ZnO nanocomposites. Therefore, different adsorption modes have been investigated for the interacting system (Fig. 12).

According to the molecular electrostatic potential (MEP), five possible optimized geometries for adsorption **N719** dye on ZnO surface were selected to understand the molecular interaction during the adsorption process.

In the monodentate linkage form of the Mode 1, one oxygen atom O32 in the carboxylic group binds to a Zn atom, in the bidentate bridging linkage form of the Mode 2, the O34 atom in the one carboxylic group binds to a Zn58 atom and the oxygen atom O34 in the other carboxylic group binds to a Zn61 atom, whereas in the bidentate chelate linkage form of Mode 3, both oxygen atoms O36 and O37 of carboxylate ion group –COO– bind to a Zn58 atom,besides, in the bidentate bridging linkage form Mode 4, the both oxygen atoms O36 and O37 in the one carboxylate ion group –COO– bind to a Zn58 atom, and the linkage also between the both oxygen atoms O38 and O39 in the one carboxylate ion group –COO– bind to the Zn61 atom and concerning the Mode 5, both oxygen atoms O38 and O39 in the carboxylate ion group –COO– bind to the Zn58 atom and the oxygen atom O36 in the carboxylic group binds to a Zn61 atom.

Among these five modes, the Mode 1 and the Mode 2 are in coincidence with the two optimized geometries modes of the adsorbed **N719** dye on the ZnO surface which recently determined by the group of De Angelis *et al.* by taking the CP method for geometry optimizations.[52] However, the other modes are attributed to the our efficient MEP method which gives more possible optimized geometries of the complex N179 dye@ZnO.

Indeed, the MEP method could be used as an efficient predictive tool to help the optimization of dye-sensitized solar cells. Through the DFT simulation, we deduced that the three optimized modes: Mode 1, Mode 2 and Mode 3 determined by the DFT simulation are agreement with the three suggested models obtained by our statistical physics models (Fig. 8(a–c)). While in this work, the DFT simulation has been determined two another possible models like Mode 4 and Mode 5 involved in the carboxylic group and the carboxylate ion groups respectively: two possible carboxylate ions groups bind onto the ZnO

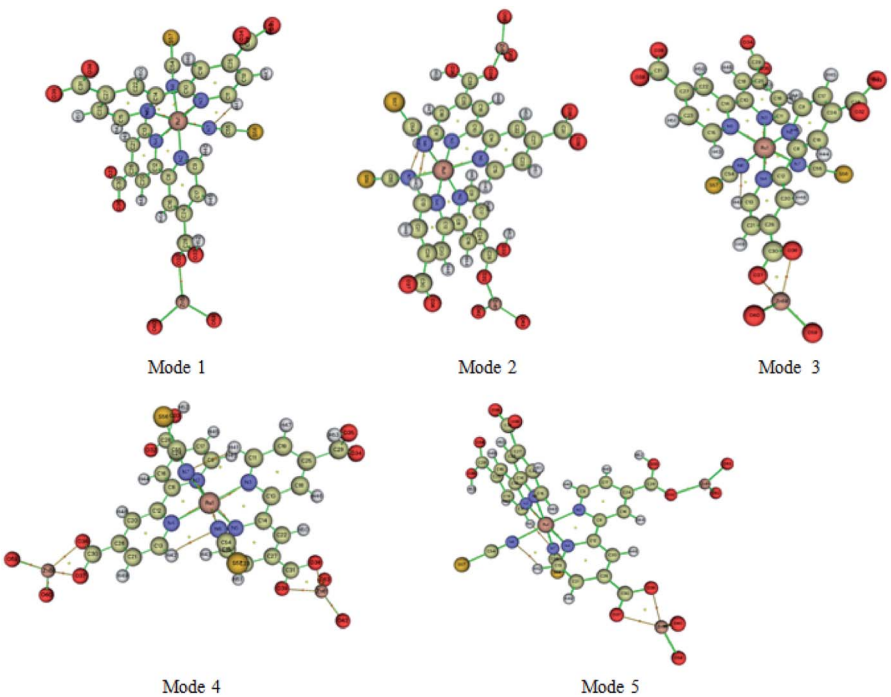

Fig. 13 AIM molecular graphic showing the different critical points (BCPs) (red small balls) and ring critical points (RCPs) (yellow small balls) of the five possible adsorption modes of **N719** dye calculated with B3LYP/6-311++G(d,p) level.

surface (Mode 4) and one of the carboxylic group associated with the carboxylate ion group to bind on the ZnO surface (Mode 5). Indeed, the DFT simulation has been completed the statistical physics modeling to determine the possible adsorption modes that could be occurred on the ZnO surface. The results of DFT simulation are in coincidence with the previously result determined by the resonant Raman scattering and infrared absorption spectroscopy which suggested that the carboxylate ion groups of the **N719** dye molecules bind to TiO_2 surface either through bidentate chelate or bidentate bridging linkages at all stages of adsorptions.[53]

7.4 AIM approach: topological parameters

Atoms-In-Molecule (AIM) method provides an effective means of mapping topological properties of the electron density to Lewis structure representation of molecules. It is the one of the most useful tools to characterize atomic and molecular interactions, particularly hydrogen bonding, is the topological analysis using the Bader theory of 'Atoms in molecules' (AIM).[54] According to AIM theory each chemical bond presents a critical point of binding denoted BCP and ring critical point RCP. The point BCP is defined as being a minimum of electronic density along the connecting path and a maximum in the other two perpendicular directions and the ring critical point RCP is represented the cyclic character of an atomic chain. Thought the location of the BCP several energetic and topological parameters can be calculated at their position in space. The calculated topological parameters are the following: the electron density r (r), the potential energy density and the interaction energy. These parameters were used to estimate the properties of the bonds in compounds and more particularly the hydrogen bonds.[55]

Molecular graphs of the **N719** dye and the ZnO using AIM2000 program are shown in Fig. 13 and the topological parameters are represented in the Table 4

From the Table 4, it seems that the values of interaction energies are ranged from −55.69 kJ mol^{-1} to −215.26 kJ mol^{-1}. The average values of interaction energies of the Mode 1, Mode 2, Mode 3, Mode 4 and Mode 5 are respectively −103.05 kJ mol^{-1}, −103.25 kJ mol^{-1}, −66.98 kJ mol^{-1}, −66.10 kJ mol^{-1} and −78.85 kJ mol^{-1}; through, this all values we noticed that the value of interaction energy of the Mode 1 is the highest value than the another values of interactions energies given by the rest of modes. According to the adsorption energies values determined by the statistical physics models, it seems that the values of interaction energies obtained by the DFT simulation are confirmed the chemisorption process of the adsorption **N719** dye on the ZnO by means the different possible five modes. Therefore, the higher values of interaction energies obtained particularly by the Mode 1 and the Mode 2 are attributed to the group carboxylic groups which provides a strong adsorption process of the **N719** dye on ZnO surface. From the Mode 2, it seems that the **N719** dye adsorbs better on the ZnO surface when two carboxylic groups are exploited than when only one is involved. Therefore, the anchorage *via* the both carboxylic group is preferred to be the best adsorption mode which can make a good stability of the system. This later is agreement with previous result that proved that the **N719** dye anchored chemically on the metal–oxide *via* two carboxylic groups and produced a good performance for dye sensitized solar cells.[27,56] De Angelis *et al.*[52] are reported that the **N719** dye is predicted to be strongly interact with the ZnO surface *via* the bidentate bridging mode. This result is in coincidence with the bidentate bridging Mode 2 obtained by the DFT simulation which reported that the **N719** dye anchored strongly on the ZnO surface *via* two carboxylic groups with a higher value of interaction energy 103.74 kJ mol^{-1} (Table 4).

Moreover, various theoretical and experimental researches have been reported that the ruthenium complexes dyes such as **N719** and N3 dyes are chemically bind by means the bidentate chelate or bridging coordination into the oxide metal surface *via* two carboxylic groups.[57,58] Furthermore, the ruthenium(II) polypyridyl complexes are among the most popular light harvesters within the solar cell community. In particular, the

Table 4 Topological parameters of AIM analysis for adsorbed **N719** dye on ZnO surface

Modes	Types		Electron density	Potential energy density V(r)	E_{int}(kJ mol^{-1})	Average value of the interaction energy E_{avg}(kJ mol^{-1})
Mode1	BCPs	O32⋯Zn58	0.05644	−0.07927	−103.05	**−103.05**
Mode2	BCPs	O34⋯Zn58	0.05639	−0.07980	−103.74	**−103.25**
		O32⋯Zn61	0.05611	−0.07904	−102.76	
Mode3	BCPs	O37⋯Zn58	0.03991	−0.04944	−64.27	**−66.98**
		O36⋯Zn58	0.04260	−0.05360	−69.68	
	NRCPs	R1	0.02727	−0.03198		
Mode4	BCPs	O37⋯Zn58	0.04260	−0.05367	−69.77	**−66.10**
		O36⋯Zn58	0.03908	−0.04822	−62.69	
		O38⋯Zn61	0.04249	−0.05352	−69.57	
		O39⋯Zn61	0.03892	−0.04798	−62.38	
	NRCPs	R1	0.02704	−0.03166	—	
		R2	0.02697	−0.03155		
Mode5	BCPs	O37⋯Zn58	0.04616	−0.05917	−76.92	**−78.85**
		O37⋯Zn58	0.03552	−0.04284	−55.69	
		O37⋯Zn61	0.05688	−0.07994	−103.93	
	NRCPs	R1	0.02671	−0.03107	—	

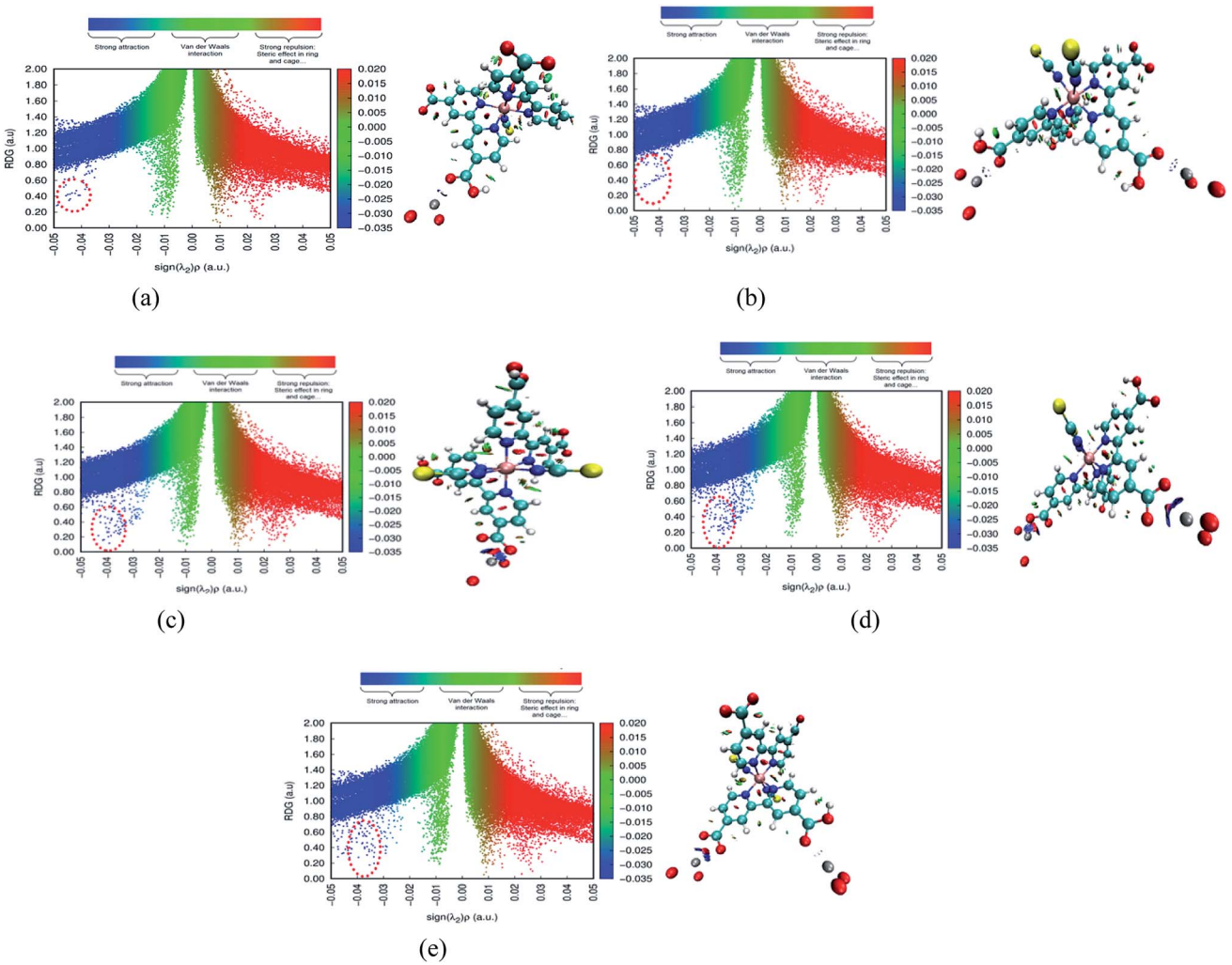

Fig. 14 The map of Reduced Densities Gradient (RDG) define the interaction modes between the **N719** dye and the ZnO surface.of the five modes: (a) RDG of Mode 1, (b) RDG of Mode 2, (c) RDG of Mode 3, (d) RDG of Mode 4 and (e) RDG of Mode 5.

prototype [*cis*-(dithiocyanato)-Ru-bis(2,2′-bipyridine-4,4′-dicarboxylate)] complex (N3) and its doubly protonated (**N719**) dye have maintained a clear lead due to their efficiency.[32,59] In this kind of compounds dyes, the bipyridine ligands ensure stable anchoring to the semiconductor surface through the carboxylic groups. In addition, the Table 4 shows also different bond and ring critical points of the five modes. The topological analysis of the five modes shows five binding critical points BCPs and three ring critical point RCPs: five BCPs (O32⋯Zn58), (O34⋯Zn58, O32⋯Zn61), (O37⋯Zn58, O36⋯Zn58), (O37⋯Zn58, O36⋯Zn58, O38⋯Zn61, O39⋯Zn61) and (O37⋯Zn58, O37⋯Zn58, O37⋯Zn561) are associated respectively to the Mode 1 the Mode 2, Mode 3, Mode 4, Mode 5, however, three RCPs are associated to the Mode 3, Mode 4 and Mode 5. Therefore, the presence of these critical points of binding BCPs were estimated the kind of binding between the adsorbate and the adsorbent by means of the value of electron density (Table 4), while, the presence of a new ring critical point RCP not only proved the stability of the system but also confirmed the cyclic character of an atomic chain. As shown in Fig. 13, the interactions between the oxygen atom of the **N719** dye and the oxygen atom of the ZnO material *via* both carboxylates ion groups give rise to the both rings NRCP1 and NRCP2. Indeed, the combination of theses both rings NRCP1 and NRCP2 have been indicated more stability to the adsorption system. Moreover, it can be also observed that the Mode 5 gives rise to a significant NRCP1 which makes a good stability to the system compared to the new ring critical point RCP of the Mode 3 and Mode 4. The existence of one and two rings NRCP produced by the carboxylate ion groups during the adsorption process of **N719** dye on ZnO surface is agreement with the previous result determined by the resonant Raman scattering and infrared absorption spectroscopy which reported that the **N719** dye are anchored to the TiO_2 surface through stable bidentate chelate or bidentate bridging linkages.[52]

7.5 Reduced density gradient (RDG)

In order to validate the results of the strong interaction of the **N719** dye on the ZnO surface obatained by the statistical physics models and the DFT simulation, the existing of intermolecular interaction was also was carried out by a RDG plot analysis and

isosurface of interactions by using the multi-wave function analysis. The results were performed and plotted respectively by the use of Multiwfn and VMD programs.[60,61] The RDG approach is a dimensionless elementary amount obtained from the density and its first derivative developed by Johnson *et al.*[62] The RDG is defined as:

$$\mathrm{RDG} = \frac{1|\nabla p(r)|}{2(3\pi^2)p(r)^{4/3}}$$

Based on the density $r(r)$ against sign λ we have tried to understand and indicate the nature of strength of the different interactions between the **N719** dye and the ZnO structure:

- If $\lambda < 0$: Attractive and binding interactions (strong interaction).

- If $\lambda > 0$: repulsive and non-binding interactions (steric effect inring and cage).

- Values close to zero indicating van der Waals interactions

The diagram RDG represents three regions of interactions: the interactions appear in the form of green plates are attributed to Van der Waals interactions; the red plates is related to the repulsive interactions which show a strong steric effect and the blue pates is attributed to the strong interaction. The results were collected in Fig. 14.

Therefore, the result shows that the diagrams RDG of the all modes exhibits the blue color of plates which proved the existence of the strong interaction intermolecular between the **N719** dye and the ZnO material. These strong interactions appear as zones marked by red circles in each mode. From Fig. 14, a clear blue spots have been checked particularly in the bidentate chelate linkage of carboxylate ion group –COO– involved in Mode 3, Mode 4 and Mode 5 (Fig. 14(c)–(e)). These modes show a significant strong attractive interaction compared to the Mode 1 and the Mode 2 which attributed to the bidentate chelate linkage modes. Moreover, the result of RDG is agreement with the result of the MEP in its identification of the geometric optimization and the AIM topological. It confirmed also the existence of strong intermolecular interaction between the **N719** dye and the ZnO surface *via* the carboxylic group which determined by the statistical physics models.

8. Conclusion

In this work we have applied two computational approaches which combine statistical physics theory and the DFT theory to study the adsorption process of **N719** dye on ZnO nanopowders and ZnO nanorods at three different deposition times of (EPD) for dye sensitized solar cells. The statistical physics models has been used to model the adsorption isotherms of **N719** dye on ZNP and ZNP materials by means of statistical physics treatment. Five models were used for fitting the experimental isotherms data of adsorption. The adsorption isotherms were well described by a monolayer model with three types of sites. The energetic parameters showed that the **N719** dye molecules anchored chemically on the ZNP and ZNR surface *via* the carboxylic groups. The DFT simulation has been used to predict reactive sites for electrophilic and nucleophilic attack for the complex **N719**@ZnO by using the molecular electrostatic potential (MEP) at the B3LYP/6-311++G(d,p). The calculations of MEP reveal five possible optimized geometric of the adsorbed **N719** dye on ZnO surface. The intermolecular interactions between the **N719** dye and the ZnO surface has been studied by using the topological AIM and reduced density gradient RDG. The result of the MEP, topological AIM and RDG are in agreement with the result of statistical physics and confirmed that the **N719** dye is chemically bonding on the ZnO surface with strengthened interaction energy *via* two carboxylic groups of bidentate bridging configuration. The excellent agreement of the computational approach DFT with a statistical physics theory indicates that the both approaches of this work could be used as an efficient predictive tool to help the optimization of dye-sensitized solar cells.

Conflicts of interest

There are no conflicts to declare.

Appendix A

Nomenclature

z_{gc}	Grand canonical partition function of one site
Z_{gc}	Total grand canonical partition function of N_m sites
β	Boltzmann factor
μ	Chemical potential of the adsorbate state
h	Plancks constant
K_B	Boltzmann constant
T	Temperature in K
C_s	The saturation dye concentration
C	The concentration of dye molecules
$C_{1/2}$	The concentration at half saturation
C_1	The concentration at half saturation for the first receptor site
C_2	The concentration at half saturation for the second receptor site
C_3	The concentration at half saturation for the third receptor site
N_o	The average number of occupied sites
N_i	The state of occupation number
Z_{tr}	The translation partition function per unit of volume
$-\varepsilon_1$	The adsorption energy of first receptor site
$-\varepsilon_2$	The adsorption energy of second receptor site
$-\varepsilon_3$	The adsorption energy of third receptor site
n_1	The number of molecules per site of first site
n_2	The number of molecules per site of second site
n_3	The number of molecules per site of third site
N_{m1}	Density of first receptor sites
N_{m2}	Density of second receptor site
N_{m3}	Density of third receptor site
J	Grand potential
Q	The adsorbed quantity

Appendix B

Treatment of model analytical expressions used to fitting

Particular model: identical sites model (homogenous and monolayer process or Hill model).

In the following we suppose that all the receptor sites are identical which corresponds to a homogenous adsorption process.

The grand canonical partition function in this case, for only one site, has the form

$$z_{gc}(T,\mu) = \sum_{N_i=0,1} e^{-\beta(-\varepsilon-\mu)N_i} = 1 + e^{\beta(\varepsilon+\mu)} \quad (A1)$$

The average number of occupied sites, can be written as:

$$N_o = \frac{N_m}{1+\left(\frac{C_{1/2}}{C}\right)^n} \quad (A2)$$

Using the eqn (7) we obtain the expression of the adsorbed quantity of the dye *versus* concentration

$$Q = \frac{nN_m}{1+\left(\frac{C_{1/2}}{C}\right)^n} \quad (A3)$$

The Langmuir model is a particular case of the Hill model, n takes the value of the unit

So its expression is:

$$Q = \frac{nN_m}{1+\left(\frac{C_{1/2}}{C}\right)^n} \quad (A4)$$

Monolayer model with two energies

We suppose that the adsorption onto the first type is carried out with an energy $(-\varepsilon_1)$ and onto the second type with an energy $(-\varepsilon_2)$. In this case, the total grand canonical partition function can be written as follows if we consider the two sites are independent:

$$Z_{total} = (z_{1gc})^{N_{m1}}(z_{2gc})^{N_{m2}} \quad (A5)$$

with z_{1gc} and z_{2gc} being the partition functions of the two types of site; they are expressed by the following relations:

$$z_{1gc} = \sum_{N_i=0,1} e^{-\beta(-\varepsilon_1-\mu)N_i} = 1 + e^{\beta(\varepsilon_1+\mu)} \quad (A6)$$

$$z_{2gc} = \sum_{N_i=0,1} e^{-\beta(-\varepsilon_2-\mu)N_i} = 1 + e^{\beta(\varepsilon_2+\mu)} \quad (A7)$$

where μ are the chemical potential son site, respectively, and N_i is the number of occupation.

Using the previous definition of occupation number, the total number of occupied sites is:

$$N_o = \frac{N_{m1}}{1+\left(\frac{C_1}{C}\right)^{n_1}} + \frac{N_{m2}}{1+\left(\frac{C_2}{C}\right)^{n_2}} \quad (A8)$$

The number of adsorbed molecules of dye *versus* the concentration is:

$$Q = \frac{n_1N_{m1}}{1+\left(\frac{C_1}{C}\right)^{n_1}} + \frac{n_2N_{m2}}{1+\left(\frac{C_2}{C}\right)^{n_2}} \quad \text{(Model 2)} \quad (A9)$$

Monolayer model with four energies

We developed this model by applying the same method.

The partition functions of the four types of the site are expressed by the following relations:

$$z_{1gc} = \sum_{N_i=0,1} e^{-\beta(-\varepsilon_1-\mu)N_i} = 1 + e^{\beta(\varepsilon_1+\mu)} \quad (A10)$$

$$z_{2gc} = \sum_{N_i=0,1,2} e^{-\beta(-\varepsilon_2-\mu)N_i} = 1 + e^{\beta(\varepsilon_2+\mu)} \quad (A11)$$

$$z_{3gc} = \sum_{N_i=0,1,2,3} e^{-\beta(-\varepsilon_3-\mu)N_i} = 1 + e^{\beta(\varepsilon_3+\mu)} \quad (A12)$$

$$z_{4gc} = \sum_{N_i=0,1,2,3,4} e^{-\beta(-\varepsilon_4-\mu)N_i} = 1 + e^{\beta(\varepsilon_4+\mu)} \quad (A13)$$

The adsorbed quantity of dye *versus* the concentration is represented as follows

$$Q = \frac{n_1N_{m1}}{1+\left(\frac{C_1}{C}\right)^{n_1}} + \frac{n_2N_{m2}}{1+\left(\frac{C_2}{C}\right)^{n_2}} + \frac{n_3N_{m3}}{1+\left(\frac{C_3}{C}\right)^{n_3}} + \frac{n_4N_{m4}}{1+\left(\frac{C_4}{C}\right)^{n_4}} \quad \text{(Model 4)} \quad (A14)$$

Double layer with one energy

The partition function of the double layer with one energy is expressed by the following relation:

$$z_{gc}(T,\mu) = \sum_{N_i=0,1,2} e^{-\beta(-\varepsilon-\mu)N_i} = 1 + e^{\beta(\varepsilon+\mu)} + e^{2\beta(\varepsilon+\mu)} \quad (A15)$$

The adsorbed quantity of dye *versus* the concentration is represented as follows

$$Q_a = nN_m\frac{\left(c/c_{1/2}\right)^n + 2\left(c/c_{1/2}\right)^{2n}}{1+\left(c/c_{1/2}\right)^n + \left(c/c_{1/2}\right)^{2n}} \quad (Model\ 5) \quad (A16)$$

Double layer with two energies

The partition function of the double layer with two energies is expressed by the following relation:

$$z_{gc}(T,\mu) = \sum_{N_i=0,1,2} e^{-\beta(-\varepsilon-\mu)N_i} = 1 + e^{\beta(\varepsilon_1+\mu)} + e^{\beta(\varepsilon_1+\varepsilon_2+2\mu)} \quad (A17)$$

The adsorbed quantity of dye *versus* the concentration is represented as follows

$$Q = nN_m \frac{\left(\frac{C}{C_1}\right)^n + \left(\frac{C}{C_2}\right)^{2n}}{1 + \left(\frac{C}{C_1}\right)^n + \left(\frac{C}{C_2}\right)^{2n}} \quad \text{(Model 6)} \qquad \text{(A18)}$$

References

1 Y. M. Meng, Y. Lin and J. Y. Yang, *Appl. Surf. Sci.*, 2013, **268**, 561.
2 X. Fang, M. Li, K. Guo, Y. Zhu, Z. Hu and X. Liu, *Electrochim. Acta*, 2012, **65**, 174.
3 P. G. Antonio, D. M. Hans, S. Helmut and S. Wilhelm, *Br. J. Nutr.*, 2003, **89**, 787.
4 H.-J. Kim, Y.-T. Bin, S. N. Karthick, K. V. Hemalatha, C. Justin Raj, S. Venkatesan, S. Park and G. Vijayakumar, Natural dye extracted from Rhododendron species flowers as a photosensitizer in dye sensitized solar cell, *Int. J. Electrochem. Sci.*, 2013, **8**, 6734–6743.
5 G. G. G. M. N. Hemamali and G. R. A. Kumara, Dye-sensitized solid state solar cells sensitized with natural pigment extracted from the grapes, *Int. J. Sci. Res.*, 2013, **3**, 1 e3.
6 Y. Chiba, A. Islam, Y. Watanab, R. Komiya, N. Koide and L. Han, Dye-sensitized solar cells with conversion efficiency of 11.1%, *Jpn. J. Appl. Phys.*, 2006, **45**, l638–l640.
7 S. Hao, J. Wu, Y. Huang and J. Lin, Natural dyes as photosensitizers for dye- sensitized solar cell, *Sol. Energy*, 2006, **80**(2), 209e214.
8 M. Gratzel, *J. Photochem. Photobiol. C Photochem. Rev.*, 2003, **4**, 145.
9 O. Carp, C. L. Huisman and A. Reller, *Prog. Solid State Chem.*, 2004, **32**, 33.
10 E. Hendry, M. Koeberg, B. O'Regan and M. Bonn, *Nano Lett.*, 2006, **6**, 755.
11 J. B. Baxter and C. A. Schmuttenmaer, *J. Phys. Chem. B*, 2006, **110**, 25229.
12 I. Corni, M. P. Ryan and A. R. Boccaccini, *J. Eur. Ceram. Soc.*, 2008, **28**, 1353–1367.
13 A. R Boccaccini, J. A. Roether, B. J. C. Thomas, M. S. P. Shaffer, E. Chavez, E. Stoll and E. J. Minay, *J. Ceram. Soc. Jpn.*, 2006, **114**, 1–14.
14 W. Sugimoto, O. Terabayashi, Y. Murakami and Y. Takasu, *J. Mater. Chem.*, 2002, **12**, 3814–3818.
15 X. Zhang and W. Yang, *Chem. Lett.*, 2007, **36**, 1228–1229.
16 O. Van der Biest and L. Vandeperre, *Annu. Rev. Mater. Sci.*, 1999, **29**, 327–352.
17 F. Hirose, K. Kuribayashi, T. Suzuki, Y. Narita, Y. Kimura and M. Niwano, *Electrochem. Solid State Lett.*, 2008, **11**, 109.
18 F. Hirose, K. Kuribayashi, M. Shikaku, Y. Narita, Y. Takahashi, Y. Kimura and M. Niwano, *J. Electrochem. Soc.*, 2009, 156–987.
19 P. Marquet, G. Andersson, A. Snedden, L. Kloo and R. Atkin, *Langmuir*, 2010, **26**, 9612–9616.
20 R. Sch€olin, M. Quintana, E. M. J. Johansson, M. Hahlin, T. Marinado, A. Hagfeldt and H. Rensmo, *J. Phys. Chem. C*, 2011, **115**, 19274–19279.
21 L. Ellis-Gibbings, V. Johansson, R. B. Walsh, L. Kloo, J. S. Quinton and G. G. Andersson, *Langmuir*, 2012, **28**, 9431–9439.
22 P. Song, Y. Z. . Li, F. C. . Ma and M. T. . Sun, *J. Mater. Chem. C*, 2015, **3**, 4810–4819.
23 S. Ranjitha, G. Rajarajan, T. S. Gnanendra, P. M. Anbarasan and V. Aroulmoji, *Spectrochim. Acta Mol. Biomol. Spectrosc.*, 2015, **149**, 997–1008.
24 A. Ben Lamine and Y. Bouazra, *Chem*, 1997, **22**, 67–65.
25 N. Bouaziz, M. Ben Manaa and A. Ben Lamine, *Phys. B*, 2017, **525**, 46–59.
26 N. Bouaziz, M. Ben Manaa and A. Ben Lamine, *Results Phys.*, 2018, **9**, 1323–1334.
27 M. Ben Manaa, B. Schmaltz, M. Bouaicha, F. Tran Van and A. B. . Lamine, *Sol. Energy*, 2016, **135**, 177–187.
28 M. Ben Manaa, B. Schmaltz, N. Bouaziz, F. Tran Van and A. B. . Lamine, *J. Alloys Compd.*, 2018, **765**, 385–395.
29 M. Ben Manaa, N. Bouaziz, B. Schmaltz, F. Tran and A. Ben Lamine, *Microporous Mesoporous Mater.*, 2018, **270**, 82–92.
30 M. Ben Manaa, N. Issaoui, N. Bouaziz and A. Ben Lamine, *J. Mater. Res. Technol.*, 2020, **9**, 1175–1188.
31 N. Bouaziz, M. Ben Manaa, F. Aouaini and A. Ben Lamine, *Mater. Chem. Phys.*, 2019, **225**, 111–121.
32 M. K. Nazeeruddin, F. De Angelis, S. Fantacci, A. Selloni, G. Viscardi, P. Liska, S. Ito, B. Takeru and M. Gratzel, *J. Am. Chem. Soc.*, 2005, **127**, 16835–16847.
33 M. K. Nazeeruddin, A. Kay, I. J. Rodicio, R. Humphry-Baker, E. Mueller, P. Liska, N. Vlachopoulos and M. Gratzel, *J. Am. Chem. Soc.*, 1993, **115**, 6382–6390.
34 A. Amat and F. De Angelis, *Phys. Chem. Chem. Phys.*, 2012, **14**, 10662–10668.
35 M. M. Hedrick, M. L. Mayo, E. Badaeva and S. Kilina, *J. Phys. Chem. C*, 2013, **117**, 18216–18224.
36 Y. Hara, M. T. Tejedor, K. Lara, D. Lubin, L. J. Brzozowski, D. J. Severseike and M. A. Anderson, *Int. J. Electrochem. Sci.*, 2013, **8**, 6734–6743.
37 S. Knani, M. Mathlouthi and A. Ben Lamine, *Food Biophys.*, 2007, **2**, 183–192.
38 N. Bouaziz, M. Ben Manaa, B. Mohamed and A. Ben Lamine, *Mol. Phys.*, 2020, **118**, 1362–3028.
39 N. Bouaziz, M. Ben Manaa and A. Ben Lamine, *Results Phys.*, 2018, **9**, 1323–1334.
40 N. Faal Hamedani and F. Farzaneh, *J. Sci. Islam. Repub. Iran*, 2006, **9**, 231–234.
41 W. A. Patrick and N. F. Eberman, *J. Phys. Chem.*, 1925, **29**, 220–228.
42 W. A. Patrick and D. C. Jones, *J. Phys. Chem.*, 1925, **29**, 1–10.
43 F. J. Luque, J. M. . Lopez and M. Orozco, *Theor. Chem. Acc.*, 2000, **103**, 343–345.
44 R. I. Dennington, T. Keith and J. Millam, *GaussView, Version 5.0.8*, Semichem. Inc, Shawnee Mission, KS., 2008, vol.12, pp. 34–36.
45 M. J. Frisch, G. W. Trucks, H. B. Schlegel, G. E. Scuseria, M. A. Robb, and D. J. Fox, *GAUSSIAN 09, Revision A.02*, Gaussian, Inc., Wallingford, CT, 2009, vol.10, pp. 122–123.
46 N. Issaoui, H. Ghalla, S. Muthu, H. T. Flakus and B. Oujia, *J. Mol. Struct.*, 2017, **1135**, 209–221.

47 N. Issaoui, H. Ghalla, S. Muthu, H. T. Flakus and B. Oujia, *Spectrochim. Acta, Part A*, 2015, **136**, 1227–1242.
48 F. De Angelis, F. Fantacci, S. Selloni, M. K. Nazeeruddin and M. Gratzel, *J. Am. Chem. Soc.*, 2007, **129**, 14156–14157.
49 B. Von Oepen, W. Kördel and W. Klein, *Chemosphere*, 1991, **22**, 285–304.
50 N. Okulik and A. H. Jubert, *Internet Electron. J. Mol. Des.*, 2005, **4**, 17–30.
51 E. Scrocco and J. Tomasi, *Adv. Quantum Chem.*, 1978, **11**, 115–121.
52 J. M. Azpiroz and F. De Angelis, *J. Phys. Chem. A*, 2014, **118**, 5885–5893.
53 K. Suto, A. Konno, Y. Kawata, S. Tasaka and A. Sugita, *Chem. Phys. Lett.*, 2012, **536**, 45–49.
54 F. Biegler-Koning, J. Schonbohm and D. Bayles, AIM2000, *J. Comput. Chem.*, 2001, **22**, 545.
55 U. Koch and P. Popelier, *J. Phys. Chem. A*, 1995, **99**, 9747.
56 J. Wang and Z. Li, *Chem. Mater.*, 2010, **22**, 579–584.
57 M. Fujihira, N. Ohishi and T. Osa, *Nature*, 1977, **268**, 226–228.
58 C. P. León, L. Lador, B. Reng and M. Thelalkat, *J. Phys. Chem. B*, 2006, **110**, 8723–8730.
59 M. K. Nazeeruddin, A. Kay, I. Rodicio, R. Humphry-Baker, E. Mueller, P. Liska, N. Vlachopoulos and M. Gratzel, *J. Am. Chem. Soc.*, 1993, **115**, 6382–6390.
60 T. Lu and F. W. Chen, *J. Comput. Chem.*, 2012, **33**, 580–592.
61 B. F. Minaev, G. V. Baryshnikov and V. A. Minaeva, *Dyes Pigm.*, 2012, **92**, 531–536.
62 E. R. Johnson, S. Keinan, P. Mori-Sanchez, J. Contreras-García, A. J. Cohen and W. Yang, *J. Am. Chem. Soc.*, 2010, **132**, 6498–6506.

